Contents lists available at ScienceDirect

South African Journal of Chemical Engineering

journal homepage: http://www.journals.elsevier.com/south-african-journal-of-chemical-engineering

Corrosion polarization behaviour and inhibition of S40977 stainless steel in benzosulfonazole/3 M H_2SO_4 solution

Roland Tolulope Loto

Department of Mechanical Engineering, Covenant University, Ota, Ogun State, Nigeria

ARTICLE INFO

Article history:
Received 18 May 2017
Accepted 21 September 2017

Keywords:
Corrosion
Inhibitor
Benzosulfonazole
Sulphuric acid

ABSTRACT

Benzosulfonazole was evaluated for its corrosion inhibition effect on S40977 stainless steel in 3 M H_2SO_4 solution through potentiodynamic polarization, open circuit potential measurement, optical microscopy and IR spectroscopy. Results obtained showed the effective performance of the compound with values of 77.33%–88.32% inhibition efficiency, at 0.25% –1.25% inhibitor concentration from electrochemical analysis. Corrosion potential value decreased from –0.359 V to –0.306 V upon addition of the compound at 0.25% concentration, which decreased progressively to –0.278 at 1.25% concentration. Identified functional groups of alcohols, phenols, amines, amides, carboxylic acids, aliphatic amines, esters and ethers within the compound completely adsorbed onto the steel from analysis of the adsorption spectra while others decreased in intensity due to partial adsorption. Thermodynamic calculations showed the cationic adsorption to be through chemisorption mechanism according to Langmuir, Freundlich and Temkin adsorption isotherms. Micro-analytical images showed a severely corroded morphology with corrosion pits in the absence of benzosulfonazole which contrast the images obtained with the inhibitor addition. The compound was determined to be mixed type inhibition.

1. Introduction

Corrosion deterioration of metallic alloys by chemical interaction with their environment is one of the major sources of overhead costs due to maintenance and repair of damaged and worn out equipment and parts in industrial plants, oil and gas refinery, marine environments, energy generating stations and ore processing. S40977 stainless steel fabricated through modification of 409 stainless steel resists mild corrosion and wet abrasion. It has been employed in applications for which aluminium, galvanized and carbon steels provide undesirable results, owing to its above average resistance to strong acids and alkalis, and cracking resulted from chloride stress corrosion. Having an average life expectancy of 5–10 times that of mild steel at considerably less cost than higher grades of stainless steel, S40977 is an effective alternative resulting in minimum capital cost increases and significant maintenance cost savings. However, unlike grade 304, S40977 steel has limited corrosion resistance in mining and mineral processing, petrochemicals and chemical, power generation, telecommunication cabinets and electrical enclosures and water and sewage treatment. Its corrosion resistance can be greatly improved with the application of a potent corrosion prevention method that boosts its life span and applicability considerably. Use of inhibitors combines the quality of been cost effective and very reliable most especially when the right chemical compound at very low concentrations give expected results (Udhayakalaa and Rajendiran,

E-mail address: tolu.loto@gmail.com.
https://doi.org/10.1016/j.sajce.2017.09.001

2015). Considerable efforts have been deployed to develop high performance corrosion inhibitors of organic origin capable of forming coordinate covalent bonds with metallic surfaces. Compounds consisting of heteroatoms containing nitrogen, oxygen, and sulphur have been reported to be effective inhibitors. These compounds have the ability to remarkably slow down the corrosion of metals and alloys by decreasing the rate of corrosion processes (Fouda et al., 2006; Udhayakala et al., 2013; Eddy and Odoemelam, 2008; Umoren et al., 2008). Benzosulfonazole, a heterocyclic compound and its derivatives are found in commercial products and in nature. It is readily substituted at the unique methyne centre in the thiazole ring. Being a thermally stable electron-withdrawing moiety, it has numerous applications in dyes, insecticides, and food flavouring agents; some drugs such as riluzole and pramipexole contain the compound. The compound has been previously investigated for corrosion inhibition for mild steel and copper in HCl and neutral chloride solutions (Ajmal et al., 1994; Rao et al., 2009; Negm et al., 2010). This research aims to study the corrosion inhibition performance of benzosulfonazole on S40977 stainless steel in 3 M H_2SO_4 acid media through electrochemical methods, corrosion potential measurement, IR spectroscopy and optical microscopy.

2. Experimental procedure

2.1. Materials and preparation

S40977 ferritic stainless steel (S40977) has a nominal composition (wt%) of 0.03% C, 1.5% Mn, 1% Si, 0.04 P, 0.015% S, 13% Cr, 1% Ni, 0.03 N and balance Fe. The steel has a cylindrical form with dimensions of 1.8 cm diameter and 1 cm length. Steel specimens were machined, abraded with silicon carbide papers (80, 320, 600, 800 and 1000 grits) before washing with distilled water and propanone, and kept in a desiccator for potentiodynamic polarization test and open circuit potential measurement according to ASTM G1-03 (2011). Benzosulfonazole obtained from BOC Sciences, USA is the organic compound for evaluation of its corrosion inhibiting properties. It is a colourless, slightly viscous aromatic heterocyclic compound with a molar mass of C_7H_5NS, g/mol. The compound was prepared in molar concentrations of 1.85×10^2, 3.70×10^2, 5.55×10^2, 7.40×10^2 and 9.25×10^2 in 200 mL of 3 M H_2SO_4 solution, prepared from analar grade of H_2SO_4 acid (98%) with deionized water.

2.2. Potentiodynamic polarization test

Polarization measurements were carried out at 30 °C ambient temperature with a three electrode system, conical glass cell containing 200 mL of the electrolyte and Digi-Ivy 2311 potentiostat. S40977 steels embedded in resin mounts with an unconcealed surface with area of 2.54 cm^2 were prepared according to ASTM G59-97 (2014). Potentiodynamic polarization curves were produced at a scan rate of 0.0015 V/s from potentials of −1 V and +1.5 V according to ASTM G102-89 (2015). Platinum rod was used as the counter electrode and silver chloride electrode (Ag/AgCl) as the reference electrode. Corrosion current density (J_{cr}, A/cm^2) and corrosion potential (E_{cr}, V) values were obtained using the Tafel extrapolation method whereby the estimated corrosion current, I_{cr}, obtained from the intercept of the two linear segment of the Tafel slope from the cathodic and anodic polarization plots (http://www.che.sc.edu/fac; http://www.ecochemie.nl/d). The corrosion rate (C_R) was calculated from the mathematical relationship;

$$C_R = \frac{0.00327 \times J_{cr} \times E_{qv}}{d} \quad (1)$$

where E_{qv} is the sample equivalent weight in grams, 0.00327 is a constant for corrosion rate calculation in mm/y (Choi et al., 2011) and d is the density in g The inhibition efficiency (η_2, %) was calculated from the corrosion rate values according to equation (2);

$$\eta_2 = 1 - \left[\frac{C_{R2}}{C_{R1}}\right] \times 100 \quad (2)$$

$C_{R1}$and C_{R2} are the corrosion rates of the uninhibited and inhibited steel specimens. Polarization resistance (R_p, Ω) was calculated from equation (3) below;

$$R_p = 2.303 \frac{B_a B_c}{B_a + B_c}\left(\frac{1}{I_{cr}}\right) \quad (3)$$

where B_a is the anodic Tafel slope and B_c is the cathodic Tafel slope, both are measured as (V vs Ag/AgCl/dec).

2.3. Infrared spectroscopy and optical microscopy characterization

BEZ/3 M H_2SO_4 solution (before and after the corrosion test) was exposed to specific range of infrared ray beams from Bruker Alpha FTIR spectrometer at wavelength range of

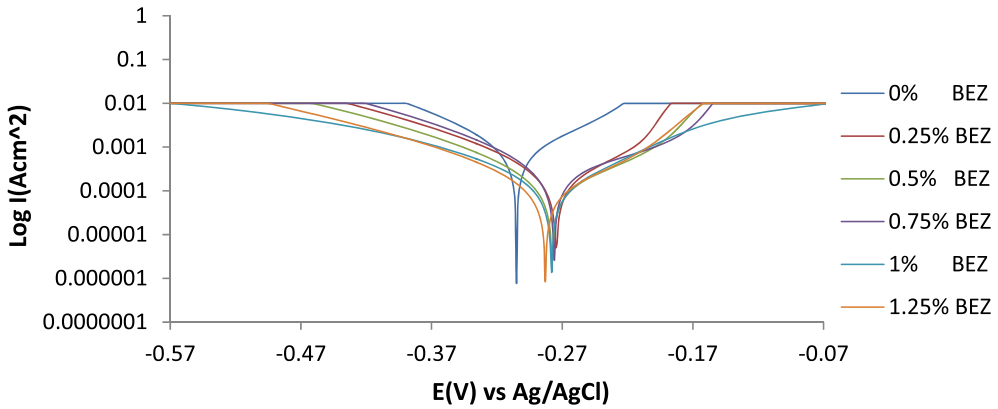

Fig. 1 – Potentiodynamic polarization curves for S40977 in 1 M H_2SO_4 (0–1.25% BEZ).

375–7500 cm^{-1} and resolution of 0.9 cm^{-1}. The transmittance and reflectance of the infrared beams at various frequencies were decoded and transformed into an IR absorption plot consisting of spectra peaks. The spectral pattern was evaluated and equated with IR absorption table to identify the functional groups responsible for corrosion inhibition. Micro-analytical images of the corroded and inhibited S40977 steel surface morphology from optical microscopy were analysed after the electrochemical test with Omax trinocular with the aid of ToupCam analytical software.

2.4. *Open circuit potential measurement*

OCP measurements were obtained at a step potential of 0.05 V/s with two-electrode electrochemical cell consisting of Ag/AgCl reference electrode and resin mounted steel specimens (exposed surface of 2.54 cm^2) as the working electrode, connected to Digi-Ivy 2311 potentiostat according to ASTM G69 – 12 (2012). The electrodes were fully immersed in 200 mL of the test media at specific concentrations of BEZ for 1800s.

3. Results and discussion

3.1. *Potentiodynamic polarization studies*

The anodic/cathodic polarization curves for S40977 3 M H_2SO_4 acid solutions are shown in Fig. 1. Experimental data on the polarization curves are presented in Table 1. The significant difference in corrosion rate values for specimen 1 at 0% BEZ and specimens 2–5 (0.25%–1.25% BEZ) in the acid media is as a result of the presence of BEZ which adsorbs on S40977 surface. Changes in corrosion rate are proportional to decrease in corrosion current and increase in polarization resistance values. BEZ addition shifts the polarization curves cathodically as shown in the corrosion potential values in Table 1, signifying a strong influence on the oxidation reactions probably through selective precipitation and adsorption on redox reaction cells on the steel surface. The cathodic shift is due to release of excess electrons which slows anodic reaction and speeds up the cathodic reaction mechanism. The effect on the cathodic polarization plot is limited though BEZ lower the slopes of the cathodic curve. Observing the anodic polarization curve, passivation behaviour is shown just after the intercept for specimen 2–5. This phenomenon is most probably due to surface coverage resulting from specific adsorption as earlier mentioned. Adsorption of BEZ molecules is marginally dependent on BEZ concentration after 0.25% BEZ from observation of the inhibition efficiency values. Values changed from 84.92% to 88.32% at 0.5%–1.25% BEZ due to strong intermolecular interaction between the protonated BEZ molecules and the valence electrons on the steel surface. The anodic Tafel slope values is as a result of the presence of surface oxides from the slow electron transfer step (Schutt and Horvath, 1987; Bockris et al., 1961; Bockris and Kita, 1961) which eventually changes due to changes in the electrode substrate, rate controlling step and influence of potential controlled conditions. The maximum change in corrosion potential value is 30 mV in the cathodic direction, thus BEZ is predominantly a mixed type inhibitor (Loto, 2017).

3.2. *IR spectroscopy analysis*

The functional groups in BEZ compound responsible for adsorption and corrosion inhibition of S40977 steel was

Table 1 – Potentiodynamic polarization data for S40977 in 3 M H_2SO_4 (0%–1.25% BEZ).

Specimen	BEZ conc. (%)	BEZ conc. (M)	S40977 corrosion rate (mm/y)	BEZ inhibition efficiency	Corrosion current (A)	Corrosion current density (A/cm^2)	Corrosion potential (V)	Polarization resistance, R_p (Ω)	Cathodic Tafel slope, B_c (V/dec)	Anodic Tafel slope, B_a (V/dec)
A	0	0	5.44	0	1.30E-03	5.13E-04	−0.305	19.74	−10.630	14.720
B	0.25	1.85E-02	1.23	77.33	2.95E-04	1.16E-04	−0.275	87.10	−10.820	27.240
C	0.5	3.70E-02	0.82	84.92	1.96E-04	7.73E-05	−0.278	130.90	−10.910	17.840
D	0.75	5.55E-02	0.75	86.13	1.81E-04	7.11E-05	−0.276	138.45	−11.260	11.230
E	1	7.40E-02	0.74	86.47	1.76E-04	6.93E-05	−0.278	145.90	−9.379	13.740
F	1.25	9.25E-02	0.64	88.32	1.52E-04	5.98E-05	−0.283	169.00	−10.360	18.850

identified through IR spectroscopy and matched with the IR table (Table of Characteristic IR Absorpions; George, 2004). The IR spectra plot of 3 M H_2SO_4/BEZ solution before and after the corrosion tests are shown in Fig. 2. The spectra plot before corrosion show peak configurations at wavelength intensities of 3338.35 cm^{-1}, 3250.77 cm^{-1}, 1631.24 cm^{-1}, 1176.77 cm^{-1}, 1102.69 cm^{-1}, 1046.76 cm^{-1} 871.55 cm^{-1} and 575.33 cm^{-1}. Matching the values with the IR table, functional groups of O–H stretch, H–bonded (alcohols, phenols), N–H stretch (amines, amides), O–H stretch (carboxylic acids), N–H bend (amines), C–H wag (–CH_2X) alkyl halides, C–N stretch (aliphatic amines), C–O stretch (esters, ethers), C–H "oop" (aromatics), C–Cl and C–Br stretch (alkyl halides) were identified within the molecular structure of BEZ. The spectra peak after corrosion show most values have decreased in intensity but signifying partial adsorption of functional groups at those peaks. The spectra peak of 3250 cm^{-1} and 1102.69 cm^{-1} (alcohols, phenols, amines, amides, carboxylic acids, aliphatic amines, esters and ethers) had completely disappeared on the peaks due to strong adsorption of these functional groups on the steel surface. This observation is responsible for the electrochemical action of BEZ in H_2SO_4 solution due to complete hydrolysis and ionization of the organic compound which formed a selective, protective film on the steel surface.

3.3. *Adsorption isotherm*

The mechanisms through which BEZ adsorbs on S40977, inhibiting the oxidation of its surface can be explained through adsorption isotherms. These mechanisms are due to the strong interaction between the steel surface and the pi-electrons within the hetero-atoms of BEZ (Zhu et al., 1988), such that BEZ is removed from the solution on contact with the steel surface. Organic adsorption from aqueous solution is relatively complex and depends on the property of the interfacial region between the steel and acid solution. It also depends on the amount and nature of surface oxide groups and functional groups, created through oxidation occurring during the activation process. A number of adsorption models have been previously applied to assess experimental results (Trasatti, 1974), however in this research Langmuir, Freundlich and Temkin adsorption isotherm produced the best fit as shown from Figs. 3–5 according to the following equations.

$$\theta = \left[\frac{K_{ads}C_{BEZ}}{1 + K_{ads}C_{BEZ}}\right] \quad (4)$$

where θ is the degree of BEZ surface coverage on 1018CS, C_{BEZ} is BEZ concentration and K_{ads} is the equilibrium constant of the adsorption mechanism. Adsorption plots of C_{BEZ}/θ vs C_{BEZ}

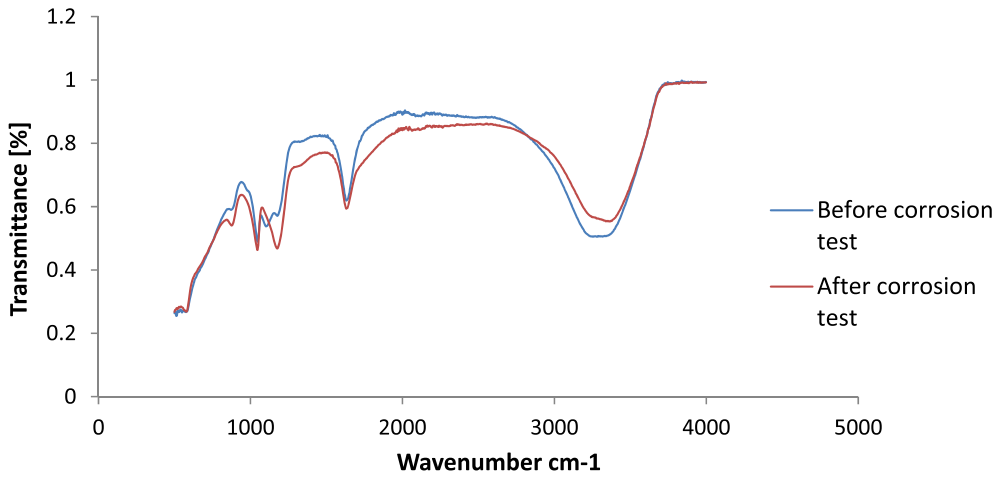

Fig. 2 – IR spectra of BEZ compound in 3 M H_2SO_4 solution before and after S40977 steel corrosion.

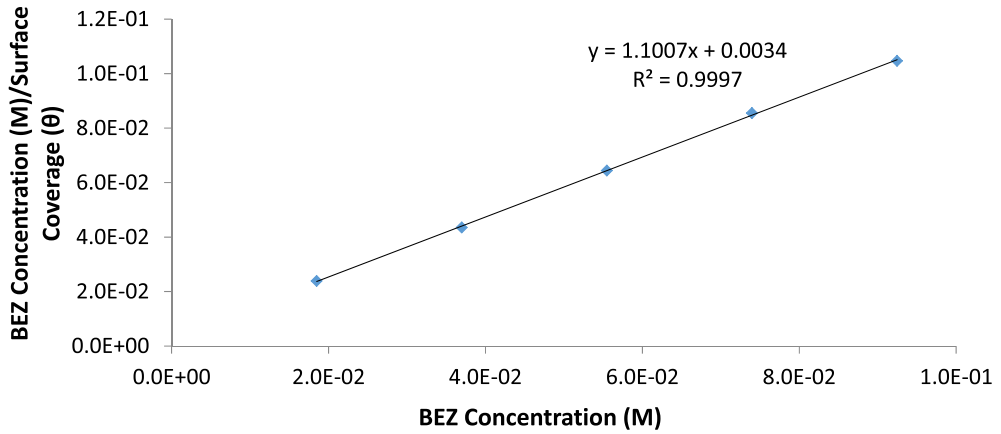

Fig. 3 – Plot of C/θ versus BEZ concentration in 3 M H_2SO_4.

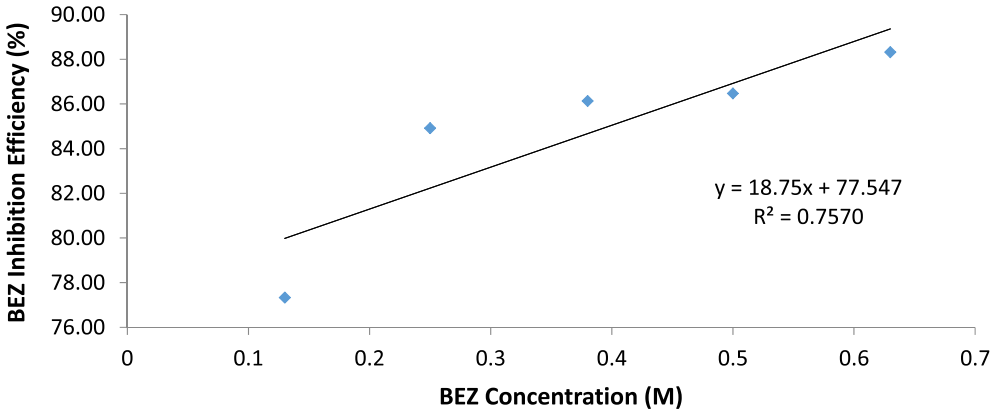

Fig. 4 – Freundlich isotherm plot of BEZ surface coverage (θ) against BEZ concentration in H_2SO_4 solution.

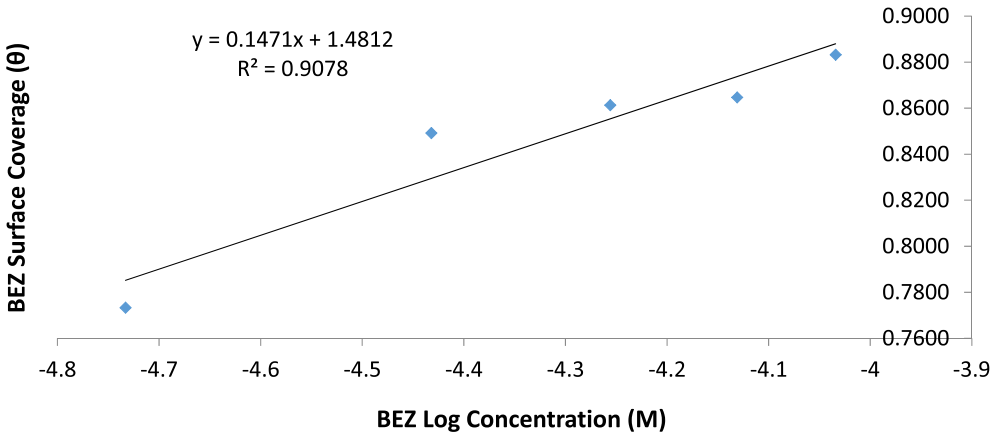

Fig. 5 – Temkin isotherm plot of BEZ surface coverage (θ) against log BEZ concentration in HCl.

strongly aligns with Langmuir adsorption isotherm (Fig. 3), having a correlation coefficient of 0.9997. Langmuir isotherm suggests single layer adsorption which occurs at definite number of reaction sites. The adsorptions are identical, equivalent and no lateral interaction between the adsorbed molecules exists (Guidelli et al., 1992).

$$\theta = KC^n \tag{5}$$

$$\log\ \theta = n\log\ C + \log\ K_{ads} \tag{6}$$

where n is a constant depending on the characteristics of the adsorbed molecule, K_{ads} is the adsorption–desorption equilibrium constant denoting the strength of interaction in the adsorbed layer. Freundlich isotherm shows the relationship between adsorbed molecules, their interaction and influence on the adsorption process through molecular repulsion or attraction. The amount adsorbed represents the sum total of adsorption on the reactive sites (Arivoli et al., 2007; Ashish and Quraishi, 2011). The correlation coefficient for Freundlich isotherm plot (Fig. 4) is 0.7570.

$$qe = B\ \ln(A + Ce) \tag{7}$$

$$\text{Where}\ \ B = RT/b \tag{8}$$

A is Temkin isotherm constant (L/g), b is the Temkin constant related to heat of adsorption, T is the temperature (K), R is the gas constant (8.314, J/mol K)and Ce is the concentration of adsorbate. B is the Temkin constant related to heat of sorption (J/mol). The Temkin isotherm assumes the heat of adsorption decreases linearly with increase in surface coverage. It is characterized by a uniform distribution of binding energies, taking into account the indirect interactions of adsorbate–adsorbate molecules on adsorption isotherm (Zeldowitsch, 1934). The Temkin isotherm plot for BEZ in H_2SO_4 (Fig. 5) had a correlation coefficient of 0.9078.

3.4. *Thermodynamics of the corrosion inhibition mechanism*

The adsorption strength of BEZ on S40977 was calculated from the thermodynamics of the inhibition mechanism. Calculated results of Gibbs free energy (ΔG^o_{ads}) for the adsorption process is shown in Table 2, and evaluated from the relationship (Aharoni and Ungarish, 1977).

$$\Delta G_{ads} = -2.303RT\ \log[55.5K_{ads}] \tag{9}$$

where 55.5 is the molar concentration of water in the solution, R is the universal gas constant, T is the absolute temperature and K_{ads} is the equilibrium constant of adsorption. K_{ads} is related to surface coverage (θ) from the Langmuir equation.

Impurities, flaws, voids, inclusions etc. on the stainless steel surface has a strong influence on the values of ΔG^o_{ads} coupled with changes in surface coverage value of BEZ (Lowmunkhong et al., 2010). The degree of cations released

Table 2 – Data for Gibbs free energy (ΔG^{o}_{ads}), surface coverage (θ) and equilibrium constant of adsorption (K_{ads}) for BEZ adsorption on S40977.

Specimen	BEZ concentration (Molarity)	Surface coverage (θ)	Equilibrium constant of adsorption (K)	Gibbs free energy, ΔG (kj mol^{-1})
1	0	0	0	0
2	1.85E-05	0.773	184,507.7	−40.00
3	3.70E-05	0.849	152,235.0	−39.52
4	5.55E-05	0.861	111,951.8	−38.76
5	7.40E-05	0.865	86,399.6	−38.12
6	9.25E-05	0.883	81,793.7	−37.98

into the solution is proportional to the degree of coverage of BEZ inhibitor. Negative values of ΔG^{o}_{ads} show the spontaneity and stability of the adsorption mechanism, with the highest of −40 kJ mol^{-1} at 0.25% BEZ and −37.98 kJ mol^{-1} at 1.25% BEZ. The values are due to the adsorption of BEZ molecules, at low BEZ concentration virtually all the molecules are adsorbed in response to oxidation reaction on the steel due to prior SO_4^{2-} adsorption. As the concentration increases not all BEZ molecules are adsorbed due to excess molecules. The values align with chemisorption adsorption mechanism involving charge sharing or transfer between the inhibitor cations and the valence electrons of the metal forming a co-ordinate covalent bond (Abiola and Otaigbe, 2008; Bouklah et al., 2006; Loto, 2016).

3.5. *Open circuit potential measurement and optical microscopy analysis*

The corrosion potential values of S40977 steel specimens at 0% BEZ to 1.25% BEZ are shown in Fig. 6. Micro-analytical images of S40977 morphology before corrosion, after corrosion without BEZ and in the presence of BEZ are shown from Figs. 7(a) to 9(b) at mag. ×40 and ×100. The morphology of the steel before corrosion [Fig. 7(a) and (b)] shows a surface mildly polished with serrated edges due to machining. In the presence of SO_4^{2-} ions without BEZ compound, the steel surface undergoes mild to severe oxidation [Fig. 8(a)], resulting in the formation of surface oxides on the steel. This observation corresponds with the corrosion potential values

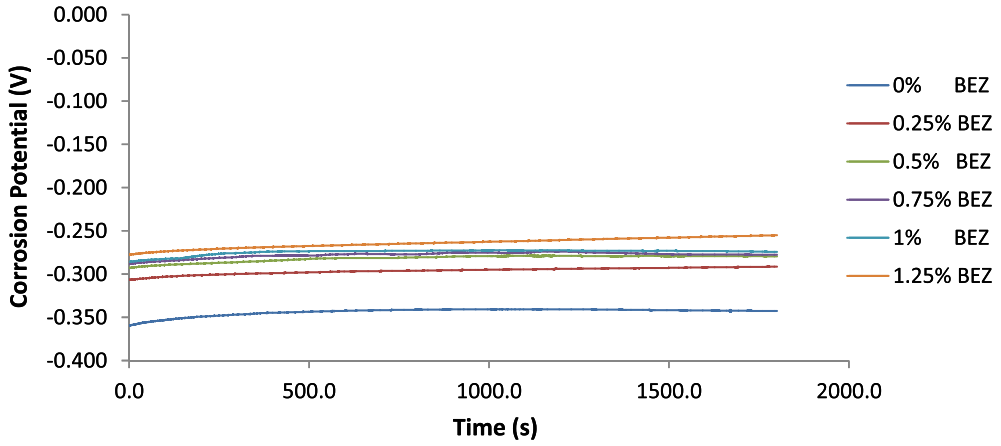

Fig. 6 – Plot of S40977 corrosion potential versus exposure time in 3 M H_2SO_4/(0%–1.25% BEZ).

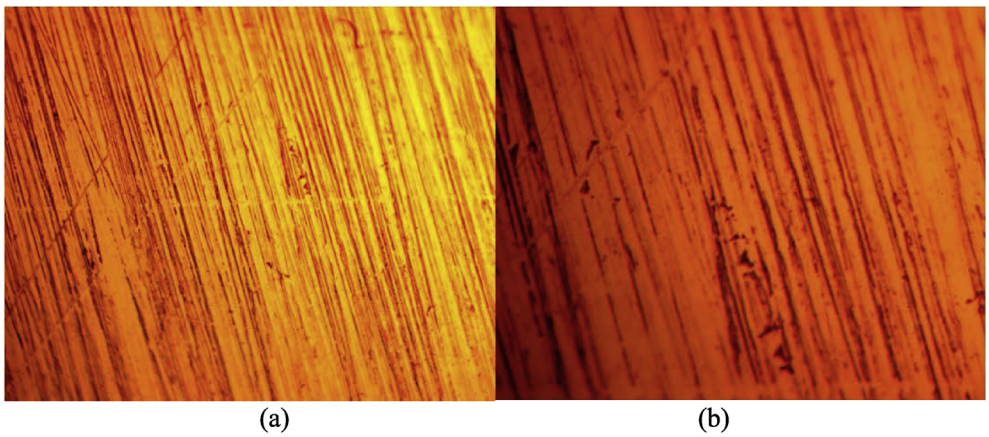

Fig. 7 – Micro-analytical image of S40977 before corrosion (a) mag. ×40, (b) mag. ×100.

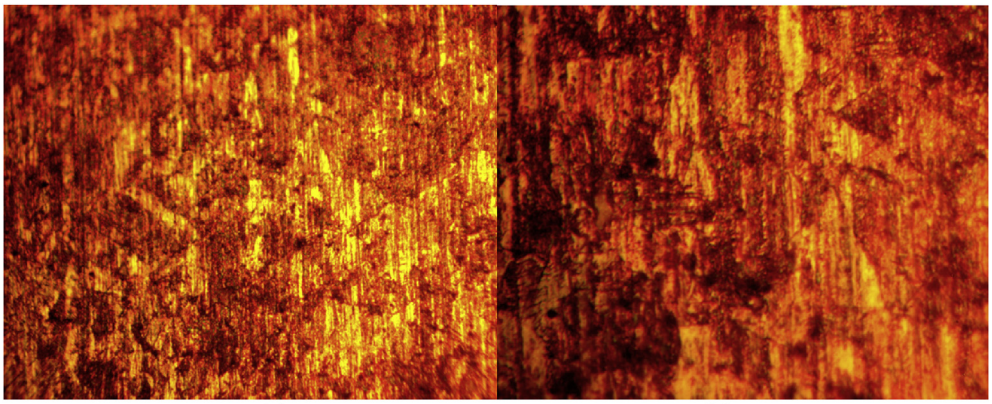

Fig. 8 – Micro-analytical image of S40977 after corrosion in 3 M H_2SO_4 without BEZ (a) mag. ×40, (b) mag. ×100.

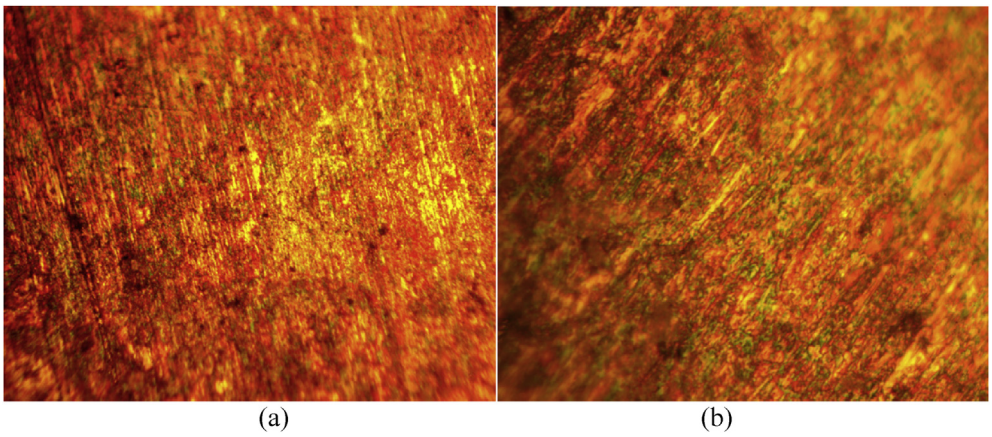

Fig. 9 – Micro-analytical image of S40977 after corrosion in 3 M H_2SO_4 with BEZ (a) mag. ×40, (b) mag. ×100.

of S40977 steel at 0% BEZ which starts at −0.359 V to −0.343 V at 1800s. Comparing the corrosion potential values to values at 0.25% BEZ, a significant decrease in corrosion potential is observed (−0.307 V to −0.293 V). At mag. ×100 [Fig. 8(b)] formation of corrosion pits is visible from breakdown of the passive film at preferential sites (flaws, impurities, inclusions etc.) as a result of anodic dissolution, resulting from the electrochemical action of SO_4^{2-} ions within the acid solution. This further accelerates the corrosion rate of the steel (Deyab, 2007). Micro-analytical images of S40977 morphology after corrosion in the presence of BEZ [Fig. 9(a) and (b)] contrasts the images after corrosion without BEZ due to the effective inhibiting action of molecules. The protonated molecules adsorbed onto the steel due to electrostatic attraction from pre-adsorbed SO_4^{2-} ions on the steel surface, hindering the anodic dissolution of the steel. The presence of corrosion pits is completely absent on the morphology of the steel. Comparing the images [Fig. 9(a) and (b)] to the corrosion potential values of S40977 steel after 0.25% BEZ, the corrosion potential decreased further in the range of −0.293 V, −0.288 V and −0.286 V at 0s to −0.280 V, −0.278 V and −0.274 V at 1800 s due to the increased action of BEZ molecules with respect to concentration. At 1.25% BEZ, there is a further significant decrease in corrosion potential (−0.278 V at 0 s to − 0.255 V 1800 s). More BEZ molecules are adsorbed on the steel surface at higher BEZ concentrations, leading to greater surface coverage (Rao and Singhal, 2009). This is in effect results in the formation of a more protective, adherent film that sufficiently hindered the access of corrosive ions to the metal surface.

4. Conclusion

BEZ effectively inhibited the corrosion and surface oxidation of S40977 steel in dilute H_2SO_4 acid solution from observation through electrochemical analysis and corrosion potential monitoring. The compound selectively adsorbed onto the steel surface through chemisorption mechanism according to the Langmuir, Freundlich and Temkin adsorption isotherm. Pre-adsorption of the steel by corrosive anions and protonation of the inhibitor functional group caused a strong electrostatic attraction leading to a well passivated steel surface. The optical image of the inhibited steel specimen significantly contrasts the image without BEZ.

Acknowledgement

The author acknowledges Covenant University Ota, Ogun State, Nigeria for the sponsorship and provision of research facilities for this project.

References

Abiola, O.K., Otaigbe, J.O.E., 2008. Adsorption behaviour of 1-phenyl-3-methylpyrazol-5-one on mild steel from HCI solution. Int. J. Electrochem. Sci. 3, 191–198.

Aharoni, C., Ungarish, M., 1977. Kinetics of activated chemisorption. Part 2. Theoretical models. J. Chem. Soc. Faraday Trans. 73, 456–464.

Ajmal, M., Mideen, A.S., Quraishi, M.A., 1994. 2-hydrazino-6-methyl-benzothiazole as an effective inhibitor for the corrosion of mild steel in acidic solutions. Corros. Sci. 36, 79–84.

Arivoli, S., Kalpana, K., Sudha, R., Rajachandrasekar, T.E., 2007. Comparative study on the adsorption kinetics and thermodynamics of metal ions onto acid activated low cost carbon. E-J. Chem. 4 (4), 238–254.

Ashish, K.S., Quraishi, M.A., 2011. Investigation of the effect of disulfiram on corrosion of mild steel in hydrochloric acid solution. Corros. Sci. 53 (4), 1288–1297.

ASTM G1-03, 2011. Standard Practice for Preparing, Cleaning, and Evaluating Corrosion Test Specimens. http://www.astm.org/Standards/G1 (accessed 30.05.16.).

ASTM G102-89, 2015. e1. Standard Practice for Calculation of Corrosion Rates and Related Information from Electrochemical Measurements. http://www.astm.org/Standards/G31 (accessed 30.05.16.).

ASTM G59-97, 2014. Standard Test Method for Conducting Potentiodynamic Polarization Resistance Measurements. http://www.astm.org/Standards/G31 (accessed 30.05.16).

ASTM G69 – 12, 2012. Standard Test Method for Measurement of Corrosion Potentials of Aluminum Alloys. https://www.astm.org/Standards/G69.htm (accessed 30.05.16.).

Bockris, J.O., Kita, H., 1961. Analysis of galvanostatic transients and application to the iron electrode reaction. J. Electrochem. Soc. 108 (7), 676–685.

Bockris, J.O., Drazic, D., Despic, A.R., 1961. The electrode kinetics of the deposition and dissolution of iron. Electrochim. Acta 4 (2–4), 325–361.

Bouklah, M., Hammouti, B., Lagrene, M., Bentiss, F., 2006. Thermodynamic properties of 2, 5-bis(4-methoxyphenyl)-1, 3, 4-oxadiazole as a corrosion inhibitor for mild steel in normal sulfuric acid medium. Corros. Sci. 48 (9), 2831–2841.

Choi, Y., Nesic, S., Ling, S., 2011. Effect of H_2S on the CO_2 corrosion of carbon steel in acidic solutions. Electrochim. Acta 56, 1752–1760.

Deyab, M.A., 2007. Effect of cationic surfactant and inorganic anions on the electrochemical behavior of carbon steel in formation water. Corros. Sci. 49, 2315–2328.

Eddy, N.O., Odoemelam, S.A., 2008. Inhibition of the corrosion of mild steel in acidic medium by penicillin v potassium. Adv. Nat. Appl. Sci. 2 (3), 225–232.

Fouda, A.S., Al-Sarawy, A.A., El- Katori, E.E., 2006. Pyrazolone derivatives as corrosion inhibitors for C-steel in hydrochloric acid solution. Desalination 201 (1–3), 1–3.

George, S., 2004. Infrared and Raman Characteristic Group Frequencies: Tables and Charts. John Wiley & Sons, New York.

Guidelli, R., 1992. Adsorption of molecules at metal electrodes. In: Kowski, J.L., Ross, P.N. (Eds.). VCH Publishers, Inc., New York, p. 1.

http://www.che.sc.edu/faculty/popov/drbnp/ECHE789b/Corrosion%20Measurements.pdf (accessed 06.04.17.).

http://www.ecochemie.nl/download/Applicationnotes/Autolab_Application_Note_COR02.pdf (accessed 06.04.17.).

Loto, R.T., 2016. Electrochemical analysis of the corrosion inhibition properties of 4-hydroxy-3-methoxybenzaldehyde on low carbon steel in dilute acid media. Cogent Eng. 3 https://doi.org/10.1080/23311916.2016.1242107, 1242107.

Loto, R.T., 2017. Study of the synergistic effect of 2-methoxy-4-formylphenol and sodium molybdenum oxide on the corrosion inhibition of 3CR12 ferritic steel in dilute sulphuric acid. Results Phys. 7, 769–776.

Lowmunkhong, P., Ungthararak, D., Sutthivaiyakit, P., 2010. Tryptamine as a corrosion inhibitor of mild steel in hydrochloric acid solution. Corros. Sci. 52, 30–36.

Negm, N.A., Elkholy, Y.M., Zahran, M.K., Tawfik, S.M., 2010. Corrosion inhibition efficiency and surface activity of benzothiazol-3-ium cationic Schiff base derivatives in hydrochloric acid. Corros. Sci. 52, 3523–3536.

Rao, V.S., Singhal, L.K., 2009. Corrosion behavior and passive film chemistry of 216L stainless steel in sulphuric acid. J. Mater. Sci. 44 (9), 2327–2333.

Rao, B.V., Iqbal, Md, Sreedhar, B., 2009. Self-assembled monolayer of 2-(octadecylthio)benzothiazole for corrosion protection of copper. Corros. Sci. 51, 1441–1452.

Schutt, H.U., Horvath, R.J., 1987. Crude Column Overhead Corrosion Problem Caused by Oxidized Sulfur Species. NACE, Houston, Texas.

Table of Characteristic IR Absorptions. http://orgchem.colorado.edu/Spectroscopy/specttutor/irchart.pdf. (accessed 12.01.17.).

Trasatti, S., 1974. Acquisition and analysis of fundamental parameters in the adsorption of organic substances at electrodes. J. Electroanal. Chem. 53 (3), 335–363.

Udhayakala, P., Jayanthi, A., Rajendiran, T.V., Gunasekaran, S., 2013. Quantum chemical studies on some thiadiazolines as corrosion inhibitors for mild steel in acidic medium. Res. Chem. Intermed. 39 (3), 895–906.

Udhayakalaa, P., Rajendiran, T.V., 2015. A theoretical evaluation on benzothiazole derivatives as corrosion inhibitors on mild steel. Der Pharm. Chem. 7 (1), 92–99.

Umoren, S.A., Obot, I.B., Ebenso, E.E., Obi-Egbedi, N.O., 2008. Synergistic inhibition between naturally occurring exudate gum and halide ions on the corrosion of mild steel in acidic medium. Int. J. Electrochem. Sci. 3 (9), 1029–1043.

Zeldowitsch, J., 1934. Adsorption site energy distribution. Acta Phys. Chim. URSS 1, 961–973.

Zhu, J., Hartung, Th, Tegtmeyer, D., Baltruschat, H., Heitbaum, J., 1988. The electrochemical reactivity of toluene at porous Pt electrodes. J. Electroanal. Chem. 244 (1–2), 273–286.